Appl. Phys. B 68, 511–517 (1999)

Applied Physics B
Lasers
and Optics

Ultrafast electron and magnetization dynamics of thin Ni and Co films on Cu(001) observed by time-resolved SHG

U. Conrad, J. Güdde, V. Jähnke, E. Matthias

Institut für Experimentalphysik, Freie Universität Berlin, 14195 Berlin, Germany

Received: 21 December 1998

Abstract. Utilizing pump–probe second-harmonic generation (SHG) with 150-fs, 800-nm laser pulses, we investigated electron and magnetization dynamics of thin Ni and Co films on Cu(001) following optical excitation. A much longer electronic relaxation time was found for Ni films than for Ni bulk. Various degrees of magnetic breakdown were induced in Ni and Co films of different thickness, applying the variation of Curie temperature with film thickness. For Ni films systematic changes of pump fluence and substrate temperature are fully consistent with the magnetization curve valid for thermal equilibrium.

PACS: 75.70.Ak; 42.65.Ky; 78.47.+p

Following theoretical predictions [1, 2] and first experimental demonstrations [3–5], magnetically induced second-harmonic generation (MSHG) has experienced a rapid development due to its intrinsic surface and interface sensitivity down to monolayer thicknesses [6]. Today this technique has evolved into a valuable tool for studying magnetic properties of ultra-thin films [7, 8] and multilayer structures [9, 10].

Up to now, all MSHG measurements on monolayers and multilayers have been carried out in a time-integrated manner, i.e., relaxation processes of optically excited electrons and spins have not yet been investigated with this technique for such quasi-2D structures. On the other hand, the availability of femtosecond laser pulses with sufficient energy per pulse has now paved the way to attack this field of research with time-resolved pump–probe MSHG. Learning more about electron and spin relaxation in ultra-thin films is not only of fundamental interest, but appears important also for real applications. In contrast to photoemission experiments, for example, such nonlinear optical probe has in addition the sensitivity to monitor relaxation processes of buried but optically accessible interfaces. This makes time-resolved MSHG a very promising technique for investigating electron and magnetization dynamics of multilayer systems.

To our knowledge there are presently four reports in the literature [11–14] which discuss magnetization dynamics on a femtosecond time-scale. Only one of those [13] investigated the spin relaxation in films a few monolayers thick – in that case 6–12 Å Ni films on Ag(100) – by utilizing spin-resolved two-photon photoemission with femtosecond time resolution. In [11] the time-resolved *linear* Kerr effect was observed on a polycrystalline 22-nm Nickel film. *Linear* Kerr ellipticity measurements were also performed in pump–probe mode on 20-nm-thick $CoPt_3$ [14]. The only time-resolved MSHG measurements hitherto were carried out on polycrystalline bulk-Ni surfaces under normal conditions [12].

In this contribution we extend our work on time-integrated MSHG experiments on ultra-thin Ni and Co films on Cu(001) [15] into the femtosecond time-resolved domain. We report here on pump–probe measurements on such films which led to new results about ultrafast electron and magnetization dynamics following optical excitation.

1 Experiment

The experimental setup consisted of a commercial high-repetition-rate amplified Ti:sapphire laser system (Coherent Mira 900/RegA 9000) in combination with a UHV chamber for the preparation of thin films. Laser radiation entered and left the chamber through fused silica windows, hitting the film at 45° angle of incidence. The film preparation is described in detail elsewhere [15]. Films were magnetized to saturation in the film plane, perpendicular to the plane of incidence (transversal geometry), by a pair of coils in Helmholtz configuration located inside the UHV chamber. The field strength at the position of the sample was typically 14 G.

The laser amplifier was operated at 800 nm with a repetition rate of 40 kHz and delivered pulses with an energy of 4 μJ and a width of about 150 fs. The laser output was split into pump and probe pulses with an intensity ratio of 4:1. The relative delay between pump and probe pulses was adjusted by a computer-controlled delay stage with an accuracy of about 1 μm corresponding to a time resolution of ≈ 7 fs. Pump and probe pulses were both focussed by the same fused silica lens ($f = 30$ cm) onto the sample. A spot diameter of about 180 μm leads to a maximal fluence of 12 mJ/cm^2. The spatial overlap between pump and probe

pulses and the beam diameters were determined by observing the stray light reflected from the sample surface with a far-field microscope through another UHV window. The incident probe pulses were always *p*-polarized whereas the polarization of the pump pulses could be changed between *p*- and *s*-polarization by means of a half-wave plate. To change the pump fluence a calcite Glan-Taylor polarizer could be inserted into the pump beam. The reflected SHG of the probe beam was also measured *P*-polarized through a Glan-Taylor polarizer and separated from the fundamental radiation by a fused silica dispersing prism and a BG 39 color filter.

To obtain a better signal-to-noise ratio, lock-in detection at about 850 Hz was utilized. The following procedure was applied. First the probe beam was modulated with a mechanical chopper and the probe SHG intensities were measured at negative delays for opposite magnetization directions, $I_0^{\uparrow}(2\omega)$ and $I_0^{\downarrow}(2\omega)$. Then the pump beam was chopped and the pump-induced changes of the probe SHG signal, $\delta I^{\uparrow\downarrow}(2\omega, t)$, were recorded as a function of pump–probe delay. At each delay the magnetization was switched by 180° and SHG yields for opposite magnetization directions were recorded. We then form the expression

$$I^{\uparrow\downarrow}(2\omega, t) = I_0^{\uparrow\downarrow}(2\omega) + \delta I^{\uparrow\downarrow}(2\omega, t) \tag{1}$$

which describes the time dependence of the total *p*-*P* polarized SHG signal of the probe beam, provided that the lock-in phase is properly taken into account. Note that in contrast to [16], we analyze here an MSHG signal generated by chopping the pump beam. This requires a slightly different data treatment from that described in [16], which is outlined in the following section.

2 MSHG data treatment

The sensitivity of SHG to the magnetization $\boldsymbol{M}$ follows from time-reversal symmetry breaking, which leads to additional components of the nonlinear susceptibility $\chi^{(2)}$. As was first pointed out in [1], $\chi^{(2)}$ then consists of even ($\chi^{(2)}_{\text{even}}$) and odd ($\chi^{(2)}_{\text{odd}}$) contributions with respect to inversion of the magnetization direction

$$\chi^{(2)}_{\text{even}}(\boldsymbol{M}) = \chi^{(2)}_{\text{even}}(-\boldsymbol{M}), \quad \chi^{(2)}_{\text{odd}}(\boldsymbol{M}) = -\chi^{(2)}_{\text{odd}}(-\boldsymbol{M})\,. \tag{2}$$

The dependence on $\boldsymbol{M}$ of the even contribution is weak and can, in first order, be neglected, while the odd contribution is proportional to the amount of $\boldsymbol{M}$ [16, 17]:

$$\chi^{(2)}_{\text{even}}(M) = \chi^{(2)}_{\text{even},0}, \quad \chi^{(2)}_{\text{odd}}(M) = \gamma M\,. \tag{3}$$

The sum and difference of the SHG intensities for opposite magnetization directions $I^{\uparrow}(2\omega)$ and $I^{\downarrow}(2\omega)$ can then be written as [12]

$$I^{\uparrow}(2\omega) + I^{\downarrow}(2\omega) = 2I^2(\omega)\big[|A\chi^{(2)}_{\text{even},0}|^2 + |B\gamma M|^2\big], \tag{4}$$

$$I^{\uparrow}(2\omega) - I^{\downarrow}(2\omega) = 4I^2(\omega)|A\chi^{(2)}_{\text{even},0}B\gamma M|\cos\phi\,, \tag{5}$$

where $I(\omega)$ is the intensity of the fundamental light. A and B are effective Fresnel factors, and ϕ is an effective phase between even and odd contributions. It is useful to define an experimental magnetic contrast or asymmetry

$$\rho = 2\frac{I^{\uparrow}(2\omega) - I^{\downarrow}(2\omega)}{I^{\uparrow}(2\omega) + I^{\downarrow}(2\omega)} \tag{6}$$

in order to describe magnetic effects in SHG. Now, usually the odd contribution is small compared to the even one and furthermore the effective phase is expected to be close to 0° or 180° [16, 18]. Under these conditions the magnetic asymmetry can be approximated by

$$\rho \approx 4\frac{|B\gamma M|}{|A\chi^{(2)}_{\text{even}}|}\,. \tag{7}$$

For in-plane-magnetized Ni films and *p*-*P*-polarized SHG, ρ is of the order of 10% [15].

Measuring the magnetic contrast as a function of time introduces an additional parameter. In principle, the same considerations apply, except that now we start from (1) and find the sum and difference of the time-dependent SHG intensities for opposite magnetization directions normalized to the SHG intensities at negative pump–probe delay:

$$\Delta^{\pm}(t) = \frac{I^{\uparrow}(2\omega, t) \pm I^{\downarrow}(2\omega, t)}{I_0^{\uparrow}(2\omega) \pm I_0^{\downarrow}(2\omega)}\,. \tag{8}$$

Introducing (1), we can write this equation as

$$\Delta^{\pm}(t) = 1 + \frac{\delta I^{\uparrow}(2\omega, t) \pm \delta I^{\downarrow}(2\omega, t)}{I_0^{\uparrow}(2\omega) \pm I_0^{\downarrow}(2\omega)}\,. \tag{9}$$

After inserting expressions (4) and (5) into (9), neglecting terms quadratic in $\chi^{(2)}_{\text{odd}}$, considering that $\chi^{(2)}_{\text{even}}$ depends only weakly on time [proof for that can be found in Figs.3a and 3b], and assuming that the effective phase is either 0° or 180° and independent of time delay, one can show that Δ^+ and Δ^- in (9) take the forms

$$\Delta^-(t) = \frac{M(t)}{M_0}, \tag{10}$$

$$\Delta^+(t) = \frac{\left|\chi^{(2)}_{\text{even}}(t)\right|^2}{\left|\chi^{(2)}_{\text{even},0}\right|^2}\,, \tag{11}$$

where M_0 is the sample magnetization at negative delay times. Hence, according to (8) the ratio $\Delta^-(t)$ must be measured to investigate magnetization breakdown and recovery while $\Delta^+(t)$ reflects the relaxation of the electron bath.

3 Results and discussion

3.1 Ni/Cu(001)

Figure 1 shows the time evolution of pump induced relative changes $\delta I(t)/I_0$ of the probe MSHG signal for different film thicknesses at 323 K. The strong peak around zero delay is

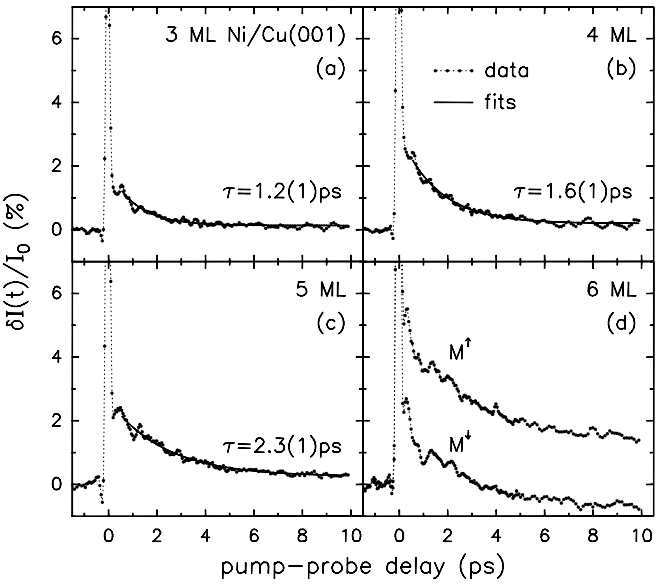

Fig. 1a–d. Relative change of the *p-P* polarized probe SHG signal as a function of pump–probe delay for 3 to 6 monolayers of Ni on Cu(001) at a substrate temperature of 323 K and *p*-polarized pump light. Curves in **a**, **b**, and **c** represent paramagnetic films. For 6 ML in **d** the Curie temperature has surpassed the substrate temperature and the probe SHG signal differs for opposite magnetization directions in transversal geometry

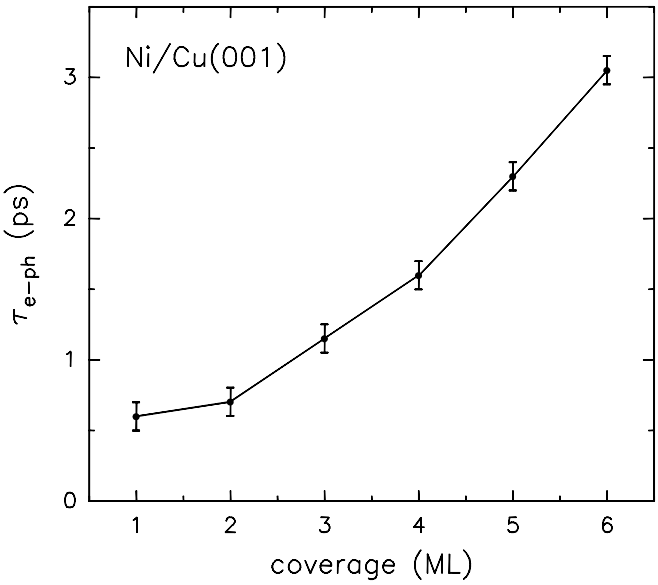

Fig. 2. Increase of electron relaxation time with thickness obtained from an exponential fit to the decay curves in Fig. 1 (errorbars originate from calculated mean deviations of the fits). Notice: the decay for a 5 ML Ni film is not shown in Fig. 1, and for 6 ML an average was used between the MSHG for $M^{\uparrow}$ and $M^{\downarrow}$

a coherent artifact resulting from a transient grating induced by interfering pump and probe beams at the sample surface. Such grating develops only for overlapping pump and probe beams with parallel polarizations [19]. The width of the peak is determined by the pulse length. When measuring at a clean Cu-surface only this correlation peak is obtained. Apart from the coherence peak, two facts show up clearly in Fig. 1: one is the decay curve at positive delays, which is more intense with increasing Ni film thickness, the other is the splitting of the signal at 6 ML when the Curie temperature of the film significantly exceeds 323 K.

With increasing film thickness the area under the decay curve grows (Fig. 1) due to increasing absorption in the Ni film. The bulk reflectivity value of Cu is ≈ 1.6 times higher than that for Ni. Using multiple reflection calculations one can estimate that half of the totally absorbed energy is deposited in the Ni film at a thickness of 7.5 ML. With growing film thickness the reflectivity drops until it reaches around 200 ML a value, which corresponds to the bulk reflectivity of Ni. The decay curve reflects the relaxation of electron temperature in the film. After optical excitation the electrons equilibrate on a timescale of typically 260–280 fs [11, 12]. During this period the lattice temperature remains effectively unchanged. Within the first few picoseconds electrons transfer energy to the lattice until both reservoirs have reached equilibrium for delay times > 5 ps. From then on the sample cools down by thermal lattice diffusion on a timescale of several hundred picoseconds. An interesting observation derived from exponential fits to the data in Fig. 1 is shown in Fig. 2. It appears that the electron phonon relaxation increases up to 6 ML thickness. We have no conclusive interpretation for such an increase, but speculate that in the beginning, for 1 and 2 ML, the electron relaxation is governed by coupling to the Cu lattice phonons. The electron relaxation time $\tau_{\text{e-ph}}$ for Cu bulk is around 700 fs [20, 21]. When the Ni films grows thicker and the electronic interface structure develops, this may form a barrier preventing the electrons to interact with the Cu substrate. On the other hand, the phonon spectrum of the film has up to 6 ML apparently not reached its full 3D character and cannot accommodate electronic energy at the same rate as for bulk Ni [12]. There are indications that the electron relaxation time peaks around 3 ps and turns faster again starting at 8 ML, but more data are needed to substantiate such dependence of $\tau_{\text{e-ph}}$ on film thickness.

The Curie temperature exceeds the substrate temperature of 323 K at about 5.4 ML [15, 22]. Thus, for 6 ML the odd tensor components of $\chi^{(2)}$ now contribute and the SHG transients differ dramatically for the two opposite directions of the external magnetic field [see Fig. 1d]. The average of these two branches, however, continues the trend of increasing absorption leading to a larger change of SHG for 6 ML. This also indicates that the odd contribution is indeed smaller than the even one [cf. (4)]. The increase with thickness of the decay time (cf. Fig. 2), on the other hand, rules out any big difference between electron and spin relaxation.

In Fig. 3 the relative sums and differences (8) of *p-P*-probe SHG signals for 7 ML Ni/Cu(001) are shown as a function of delay time. For the two curves on the left-hand side, *pump* pulses were *p*-polarized. This led to the large coherence peak in $\Delta^{+}(t)$ [Fig. 3a] which is missing for orthogonally polarized pump and probe pulses in Fig. 3b. Note that the curves indicate about twice as much absorption ($\approx 6\%$) for *p*-polarized than for *s*-polarized light ($\approx 3\%$), as expected from bulk optical constants. Hence, for identical fluences considerably higher temperatures can be reached with *p*-polarized pump pulses compared to *s*-polarized ones. The small changes of $\Delta^{+}(t)$ in Fig. 3a and b provide an upper limit for the influence of even tensor components on Δ^{-} and justify their omission leading to (10).

In Fig. 3c it can be seen that for *p*-polarized pump radiation the relative difference Δ^{-} breaks down to near zero

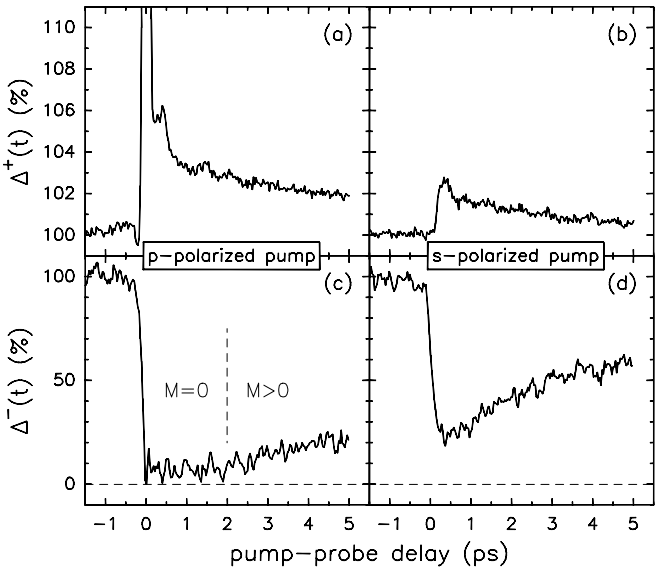

Fig. 3a–d. Relative sum $\Delta^+(t)$ (**a** and **b**) and relative difference $\Delta^-(t)$ (**c** and **d**) of the *p*-*P* probe SHG signal for opposite magnetization directions in transversal geometry as a function of pump–probe delay for 7 ML Ni/Cu(001) at 323 K. **a** and **c** show the result for *p*-polarized, **b** and **d** for *s*-polarized pump radiation, respectively. The applied pump fluence was 12 mJ/cm^2

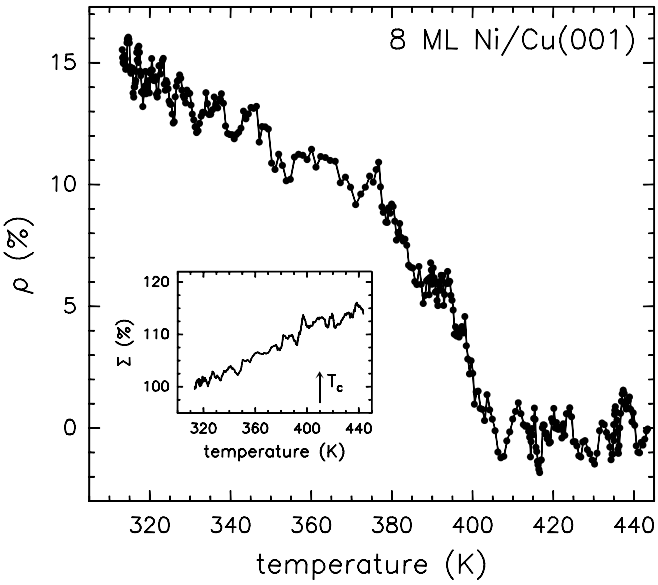

Fig. 4. Magnetization curve for annealed 8 ML Ni/Cu(001) measured in the direction of decreasing temperature. Plotted is the magnetic contrast ρ of the *p*-*P* SHG signal for opposite magnetization directions in transversal geometry as a function of substrate temperature. For this measurement the radiation of the 25 fs Ti:sapphire oscillator has been used. The *inset* shows the temperature dependence of Σ, the normalized average SHG yield for opposite magnetization directions

within the pulse width, stays quenched for about 2 ps (while Δ^+ does not saturate!) and then begins to raise again. The deviation from exactly zero originates from an uncertainty in determining the SHG yield $I_0^{\uparrow\downarrow}(2\omega)$ for negative delay times, where the probe beam had to be chopped. The fast magnetic breakdown shows that the electron temperature exceeds the Curie temperature of about 400 K [22, 23] immediately after absorption of the pump pulse. Within the experimental resolution there is no time delay between electron and spin temperature. The fact that Δ^- saturates near zero for as long as 2 ps provides clear evidence that the breakdown of Δ^- is not caused by any time dependence of the effective phase ϕ between the odd and even tensor elements [cf. (5)]. If there were a phase effect, Δ^- could also turn negative, which has never been observed in any one of our measurements. For this reason a time dependence of ϕ was disregarded in (10). This phase independence together with the neglect of residual contributions by even tensor elements make Δ^- the quantity which describes the magnetization dynamics. Hence, the curves displayed in Fig. 3c and d represent the time dependence of magnetization for 7 ML Ni films at two levels of excitation. For *p*-polarized pump light the absorption was sufficiently strong to reach an electron temperature higher than the Curie temperature. It took the electron temperature 2 ps to drop again below the Curie point and from that time on the magnetization starts to recover [Fig. 3c]. With *s*-polarized pump pulses electrons could not be heated above the Curie temperature. Therefore, the magnetization breakdown is only of the order of 80% but still as fast as in the *p*-polarized case [Fig. 3d].

To investigate the dependence of MSHG on temperature more systematically, we performed measurements as a function of substrate temperature. The temperature dependence of the magnetic contrast ρ for opposite magnetization directions in transversal geometry is plotted in Fig. 4. It represents the stationary magnetization curve of an 8 ML Ni film on Cu(001). For this measurement, a home-built Ti:sapphire oscillator delivering 25-fs, 810-nm pulses was used. At 310 K the asymmetry ρ amounts to about 15% and a Curie temperature of about 410 K can be deduced in reasonable agreement with [22, 23]. The inset in Fig. 4 shows the temperature dependence of the averaged values of the SHG signals for opposite magnetization directions normalized to the starting temperature $T_0 = 310$ K:

$$\Sigma = \frac{I^{\uparrow}(2\omega, T) + I^{\downarrow}(2\omega, T)}{I^{\uparrow}(2\omega, T_0) + I^{\downarrow}(2\omega, T_0)} \,. \tag{12}$$

In this inset plot there is no break at the Curie temperature. Comparison with (5) tells us that Σ is governed by the even contribution to $\chi^{(2)}$, providing another proof that the odd contribution in (4) is small compared to the even one. The increase of Σ with temperature is consistent with the observed increase of $\chi^{(2)}_{\text{even}}$ in pump–probe mode [see Fig. 3a and 3b].

If in a time-resolved measurement the substrate temperature is kept fixed and the pump energy is increased, one always starts at the same point on the magnetization curve (Fig. 4) but the magnetization is driven toward the Curie temperature where it vanishes. The time evolution of the relative difference between SHG signals for opposite magnetization directions is shown in Fig. 5 for four different pump fluences applied to an 8 ML Ni film. Note that the magnetization breaks down for all pump fluences within the same short time interval. For a pump energy of 0.75 μJ the breakdown amounts to $\approx 50\%$, for 1.25 μJ $\approx 75\%$ and for 1.75 μJ it reaches zero for about 0.5 ps. When the pump energy is further increased to 2.25 μJ, Δ^- vanishes during a longer period up to 1 ps. This is in good agreement with the measurements on the 7 ML Ni film in Fig. 3. That film has a somewhat lower Curie temperature and a higher pump energy was ap-

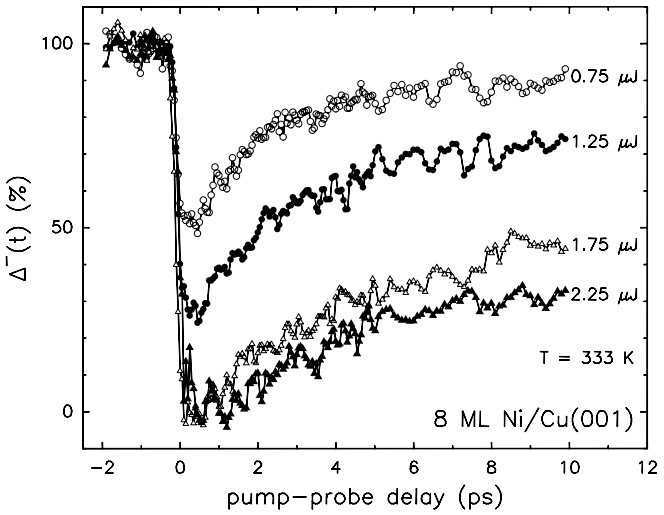

Fig. 5. Pump energy dependence of the breakdown of magnetization for 8 ML Ni/Cu(001). Plotted is the relative difference $\Delta^-(t)$ for *p*-*P* polarization as a function of pump–probe delay for different energies of the *p*-polarized pump light whereas an energy of 2.25 μJ corresponds to a fluence on the sample of about 10 mJ/cm^2. The substrate temperature was 333 K

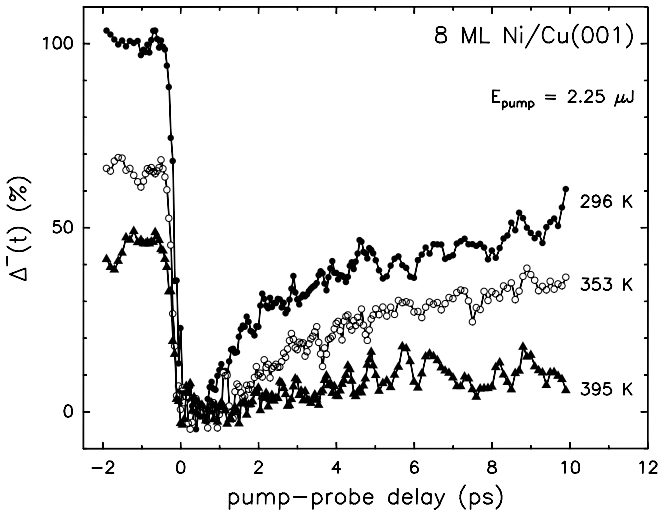

Fig. 6. Substrate temperature dependence of the breakdown of magnetization for 8 ML Ni/Cu(001). Plotted is the relative difference $\Delta^-(t)$ for *p*-*P* polarization as a function of pump–probe delay for different substrate temperatures. Here, $\Delta^-(t)$ is calculated for all curves with $(I_0^{\uparrow} - I_0^{\downarrow})$ for $T = 296$ K. The energy of the *p*-polarized pump light was 2.25 μJ

plied, so the time interval for totally quenching the magnetization was longer. The recovery of magnetization in Fig. 5 has about the same time constant for all four fluences and reaches around 10 ps levels, which reflect the degree of magnetization when electrons and lattice are in thermal equilibrium. As expected, these levels decrease with increasing pump energy according to a higher equilibrium temperature and a magnetization curve similar to the one shown in Fig. 4. A quantitative comparison between pump–probe measurements and the magnetization curve is, however, not feasible due to experimental constraints. The pump and probe beams were focused to the same size at the sample surface entailing a laterally nonuniformly heated probe area. Although SHG as a second order process probes only half of the fundamental spot size, the probe signal results from slightly different degrees of magnetization.

The magnetization dynamics of an 8 ML Ni film for a fixed pump fluence and three different substrate temperatures is displayed in Fig. 6. Here, the scale for Δ^- is defined by the fact that the pump fluence of 2.25 μJ is just sufficient to produce a complete breakdown of magnetization at a starting temperature of 296 K ($\Delta^- = 100\%$). When the substrate temperature is changed and the same pump energy is used, the curves start at different points on the magnetization curve. Hence, higher substrate temperatures imply smaller relative differences Δ^-, which show up in Fig. 6 as lower starting levels. Since the fluence is kept fixed the electron temperature overshoots the Curie point the higher the substrate temperature is. Consequently, the magnetization is then erased completely for correspondingly longer time intervals. The amount of magnetic recovery at 10 ps is also defined by the different substrate temperatures and the applied fluence in accordance with the magnetization curve.

The results presented in Figs. 5 and 6 prove two facts. (1) The fast magnetic breakdown after optical excitation is independent of fluence and substrate temperature and no time delay is observable between the establishment of an electron temperature and the loss of spin orientation. (2) Size and time duration of magnetization breakdown is fully consistent with expectations from the classical magnetization curve, emphasizing that also in ultrathin Ni films the magnetization dynamics is governed by electron temperature, in agreement with previous observations for bulk-Ni [12].

3.2 Co/Cu(001)

As a second example we examined thin Co films on Cu(001) where the magnetization lies also in the film plane but with substantially higher Curie temperatures compared to thin Ni films. Figure 7 shows the stationary magnetization curve for a 2.1 ML thick Co film on Cu(001) which exhibits a Curie temperature slightly below 500 K, in agreement with [23], and a magnetic contrast of about 30% at 345 K. The roughly 2.5 times larger asymmetry compared to Ni films at this temperature (see Fig. 4) can be understood by the ratio of magnetic moments of Co and Ni, which amounts to about 2.9 for bulk materials at 4.2 K [24]. In contrast to an 8 ML Ni film, the sum of the SHG signals for opposite magnetization directions, which is proportional to the even part of the nonlinear susceptibility, decreases with substrate temperature as shown in the inset in Fig. 7. From this trend we expect the relative sum $\Delta^+(t)$ in pump–probe mode to decrease with increasing electron temperature, as observed in Fig. 8. Again we do not see any break at the Curie temperature, although this statement is not as rigid as for Ni (Fig. 4) since interdiffusion forbids measurements at higher temperatures.

The magnetization dynamics of Co films on Cu(001) could only be examined in the very narrow thickness range between two and four monolayers. Thinner films are still paramagnetic at room-temperature and thicker films exhibit such high Curie temperatures that the available laser pulse energy was not sufficient to affect the magnetization appreciably.

A series of pump probe SHG measurements on Co films on Cu(001) carried out at 323 K is shown in Fig. 8 for thicknesses of 2, 3, and 4 ML. To eliminate the correlation peak,

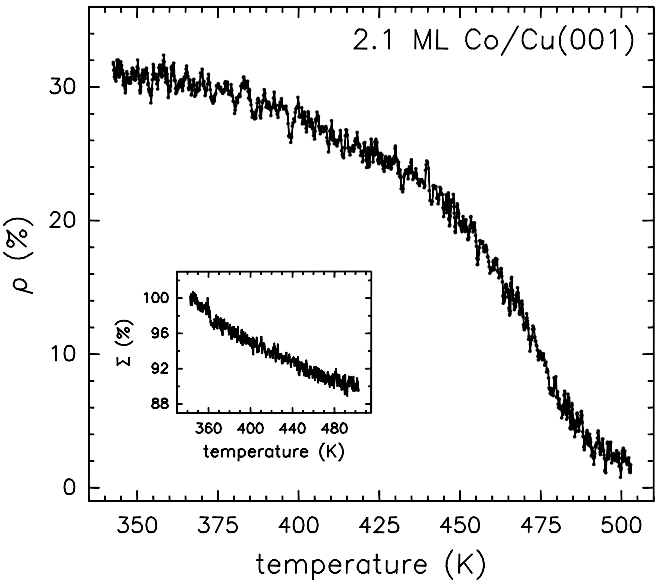

Fig. 7. Magnetization curve for annealed 2.1 ML Co/Cu(001) measured in the direction of decreasing temperature. Plotted is the magnetic contrast ρ of the *p-P* SHG signal for opposite magnetization directions in transversal geometry as a function of substrate temperature. The inset shows the temperature dependence of Σ, the normalized average SHG yield for opposite magnetization directions

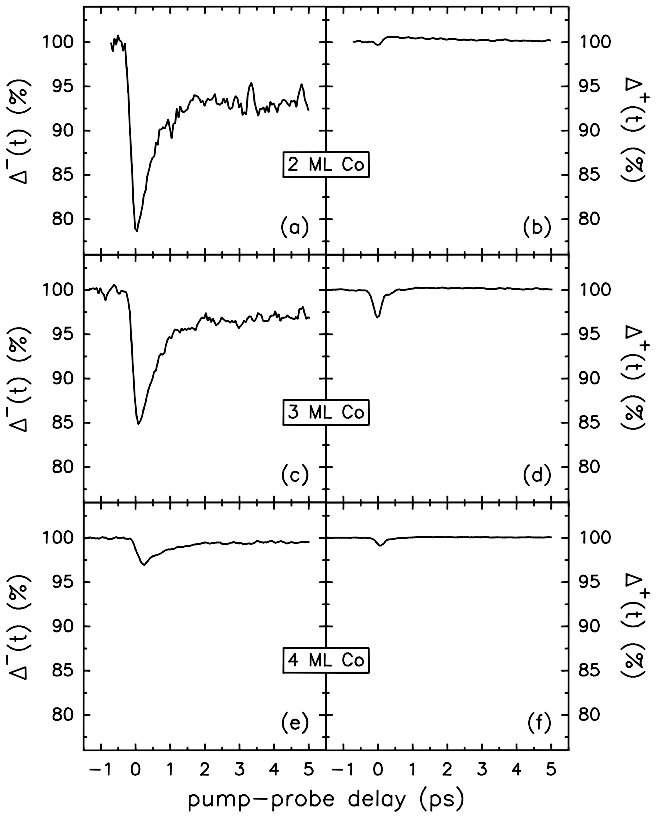

Fig. 8a–f. Relative difference $\Delta^-(t)$ (**a**, **c** and **e**) and relative sum $\Delta^+(t)$ (**b**, **d** and **f**) of the *p-P* probe SHG signal for opposite magnetization directions in transversal geometry as a function of pump–probe delay at 323 K for different Co coverages on Cu(001). **a** and **b** show the result for 2 ML Co, **c** and **d** for 3 ML Co and **e** and **f** for 4 ML Co, respectively. The pump radiation was *s*-polarized and the applied pump fluence was 10 mJ/cm^2

s-polarized pump pulses were used. The normalized differences Δ^- in Fig. 8a,c and e demonstrate the magnetization dynamics. The time response is as fast as in Ni films and the signal breaks down in an interval which is limited by the experimental time resolution. The different degrees of magnetic breakdown for equal pump fluences, compared to Ni, are due to substantially higher Curie temperatures in case of Co/Cu(001). Therefore, the effects in Figs. 8a,c and e are not as distinct as for Ni films. The rapid increase of Curie temperature with thickness is reflected in the decreasing amount of magnetization breakdown.

The normalized sums Δ^+ in Fig. 8b,d, and f show that the electron temperatures reached with the same pump fluence vary with thicknesses. Because of the strong electron–phonon coupling the response is very fast. The highest temperature is reached for 3 ML. Nevertheless it does not lead to the largest effect for the relative difference Δ^- since the Curie temperature is larger for 3 ML. Clearly, the results in Fig. 8b,d, and f are not sufficient for a more detailed interpretation and further studies of the electron relaxation of thin Co films must be carried out.

4 Conclusion

Ultrafast magnetization dynamics of thin Ni and Co films on Cu(001) has been measured by utilizing time-resolved second-harmonic generation. In both cases magnetization breaks down within the temporal width of the laser pulses of about 150 fs. The degree of magnetic breakdown was shown to decrease with increasing film thickness due to increasing Curie temperatures. In the case of 7 ML Ni/Cu(001) it was possible to totally quench the magnetization for up to 2 ps with fluences of about 12 mJ/cm^2. The fact that the magnetic contribution to the SHG can be completely erased proves that this technique is indeed sensitive to the magnetization. Measurements were performed on 8 ML Ni/Cu(001) films with systematic variations of both, pump fluence and substrate temperature. All results fully support the assumption that the magnetization curve $M(T_e)$, valid for thermodynamic equilibrium, governs the spin dynamics as soon as an electron temperature has formed. Qualitatively, we see similar effects in 2 to 4 ML Co films. However, because of the much higher Curie temperature only small magnetic effects could be induced with our fluences and the time dependence of MSHG of Co films needs further investigations.

Acknowledgements. We would like to thank Dr. J. Hohlfeld for fruitful discussions. This work was supported by the Deutsche Forschungsgemeinschaft, Sfb 290.

References

1. R.P. Pan, H.D. Wei, Y.R. Shen: Phys. Rev. B **39**, 1229 (1989)
2. W. Hübner, K.H. Bennemann: Phys. Rev. B **40**, 5973 (1989)
3. O.A. Aktsipetrov, O.V. Braginskii, D.A. Esikov: Sov. J. Quant. Electron. **20**, 259 (1990)
4. J. Reif, J.C. Zink, C.-M. Schneider, J. Kirschner: Phys. Rev. Lett. **67**, 2878 (1991)
5. J. Reif, C. Rau, E. Matthias: Phys. Rev. Lett. **71**, 1931 (1993)
6. K.-H. Bennemann (Ed.): *Nonlinear Optics in Metals*, International Series of Monographs on Physics (Oxford Press, London 1998)
7. M. Straub, R. Vollmer, J. Kirschner: Phys. Rev. Lett. **77**, 743 (1996)

8. Q.Y. Jin, H. Regensburger, R. Vollmer, J. Kirschner: Phys. Rev. Lett. **80**, 4056 (1998)
9. B. Koopmans, M.G. Koerkamp, Th. Rasing, H. van den Berg: Phys. Rev. Lett. **74**, 3692 (1995)
10. A. Kirilyuk, Th. Rasing, M.A.M. Haast, J.C. Lodder: Appl. Phys. Lett. **72**, 2331 (1998)
11. E. Beaurepaire, J.-C. Merle, A. Daunois, J.-Y. Bigot: Phys. Rev. Lett. **76**, 4250 (1996)
12. J. Hohlfeld, E. Matthias, R. Knorren, K.H. Bennemann: Phys. Rev. Lett. **78**, 4861 (1997)
13. A. Scholl, L. Baumgarten, R. Jaquemin, W. Eberhardt: Phys. Rev. Lett. **79**, 5146 (1997)
14. G. Ju, A. Vertikov, A.V. Nurmikko, C. Canady, G. Xiao, R.F.C. Farrow, A. Cebollada: Phys. Rev. B **57**, R700 (1998)
15. V. Jähnke, U. Conrad, J. Güdde, E. Matthias: Appl. Phys. B **68**, 485 (1999)
16. J. Hohlfeld, J. Güdde, U. Conrad, O. Dühr, G. Korn, E. Matthias: Appl. Phys. B **68**, 505 (1999)
17. U. Pustogowa, W. Hübner, K.H. Bennemann: Surf. Sci. **307**, 1129 (1994)
18. B. Koopmans, A.M. Janner, H.A. Wierenga, T. Rasing, G.A. Sawatzky, F. van der Woude: Appl. Phys. A **60**, 103 (1995)
19. B.S. Wherret, A.L. Smirl, T.F. Boggess: IEEE J. Quantum Electron. **QE-19**, 680 (1983)
20. J. Hohlfeld, U. Conrad, E. Matthias: Appl. Phys. B **63**, 541 (1996)
21. U. Conrad: Diplomarbeit (Fachbereich Physik, Freie Universität Berlin 1995)
22. M. Farle: Rep. Prog. Phys. **61**, 755 (1998)
23. F. Huang, M.T. Kief, G.J. Mankey, R.F. Willis: Phys. Rev. B **49**, 3962 (1994)
24. R.W. Cahn, P. Haasen, E.J. Kramer (Eds.): *Electronic and Magnetic Properties of Metals and Ceramics Part 1*, Vol 3A, Materials Science and Technology (VCH, Weinheim 1991)